Effect of unconfined compressive strength of rock on dynamic response of shallow unlined tunnel

Mohammad Zaid[1] · Md. Rehan Sadique[1] · Manojit Samanta[2]

Abstract

Tunnels and underground space have been evolved as an integrated part of sustainable transportation infrastructure of both the developed and developing countries. Tunnels also have strategic importance in the defence sector of the nation. In recent decades, tunnels have been subjected to several events of intentional and unintentional blast incidents. The present study investigates the response of shallow unlined rock tunnels subjected to an internal blast. The effect of different unconfined compressive strengths (UCS) of rock on the extent of damage produced due to blast loading has been investigated. UCS representing dolomite, shale, sandstone, granite, basalt and quartzite medium has been investigated through a three-dimensional finite element model having dimensions of 30 m × 30 m in cross section and 35 m in length generated in Abaqus. The diameter of the unlined tunnel has been taken as 5 m having overburden depth of 12.5 m. Coupled-Eulerian–Lagrangian modelling has been adopted to simulate the blast loading. Nonlinear Mohr–Coulomb failure criteria have been adopted for different rock media. Trinitrotoluene (TNT) explosive has been used to simulate the blast loading, and Jones–Wilkins–Lee material model has been adopted to model the characteristics of TNT. Subsequently, a relation has been proposed to understand the damage caused by TNT blast loading in a shallow unlined tunnel. The total induced energy due to internal blast loading has been found to be maximum and minimum in dolomite and quartzite, respectively.

Keywords Abaqus · Blast · Rock · Tunnel · Unconfined compressive strength

1 Introduction

The development of underground tunnels system has been considered as a challenging geotechnical project among all the sustainable transportation system. Blast of explosive within the tunnel causes complex loading conditions and understanding the related mechanism is essential due to the rise in such cases in recent past. The underground explosion in the Salang tunnel of Afghanistan (1982) had caused severe casualties where 1000–3000 people were dead [1]. Later, London underground metro tunnels had experienced three explosion events where 700 people were injured and 52 deaths were reported [2]. In past two decades, there has been a rise in blast-related disasters at Moscow metro tunnel (2010), Minsk metro (2011), Bayrampasa metro (2015), Saint Petersburg metro (2017) and many more [3]. Due to several uprising and insurgency in the world, tunnels have faced extreme loading events in the past few decades [3]. Therefore, blast resistant design of tunnel is necessary to prevent the casualties and strengthen the metro tunnel against blast-related disasters. The amount of explosive and the properties of the surrounding media are the necessary parameters, which govern the stability of tunnel against

✉ Md. Rehan Sadique, rehan.sadique@zhcet.ac.in; Mohammad Zaid, mohammadzaid1@zhcet.ac.in; Manojit Samanta, manojit@cbri.res.in | [1]Department of Civil Engineering, Aligarh Muslim University, Aligarh, Uttar Pradesh 202002, India. [2]Geotechnical Engineering (Division), CSIR-Central Building Research Institute, Roorkee, Uttarakhand 247667, India.

blast load [4]. Moreover, the assessment of the damage caused by an explosion in the underground tunnel is the uphill struggle due to multiple reflections of shock waves [5]. However, several scientists and researchers had studied the stability of tunnel under dynamic loading [6–18].

Several studies in the past have helped in understanding the response of tunnel in soil and rock subjected to blast loading [9, 17, 19–27]. It had been observed that the tunnels with smaller radius of curvature are suffered higher deformation and damage [5]. Moreover, it had been concluded that the compressibility of geomaterial surrounding the tunnel and the ground-tunnel interaction are the significant factors influencing the damage inside and around the tunnel [28]. Also, it had also been observed that the failure of tunnel lining and a small amount of transmission of blast energy in the tunnel were observed for a large amount of explosive [29]. Formation of large cavitation zones in the tunnel subjected to blast loading has also been observed [30]. Further, geofoam liner in the tunnel had been applied to reduce the blast damage [31]. Basalt fibre-reinforced polymer bars had been suggested as reinforcement for urban utility tunnels [32]. In case of twin tunnel, the displacement increases up a certain distance and then decreases for the tunnel subjected to blast loading [33].

Further, a numerical study of the blast had been carried out by Deng et al. [34] using UDEC for tunnel in jointed rock mass. It had been concluded that joint spacing significantly affects the disturbed zone when subjected to blast loading. Also, the bolt-supported tunnels are safer than the unsupported tunnels in jointed rock mass [34]. However, in the present study, an already treated tunnel has been considered. The effect of rock weathering in the tunnel also plays a pivotal role on the stability when subjected to internal blast loading. By using CEL method for blast simulation, it had been observed that weathering of rock has a significant consequence on the stability of the tunnel subjected to blast load [35]. Moreover, the attenuation of shock waves was observed for the rock having low modulus and a high degree of weathering. Furthermore, propagation of shock wave had been observed in rock having a lower degree of weathering. Position of the blast has a substantial effect on the behaviour of twin tunnel [20]. The deformation and damage of geomaterial and tunnel lining are dependent on the location of explosive position inside the tunnel and the radius of curvature of the tunnel [5]. Researchers also investigated the dynamic response of tunnel in weathered rock, propagation of shear wave and behaviour of rock subjected to blast loading [36–38]. Moreover, blast analysis of tunnel had been studied mostly using Ansys, LS-DYNA and Abaqus [3–5, 21, 28].

However, information related to the response of rock tunnels subjected to blast loading is still limited. Moreover, the relation between the inherent properties of rock and deformations observed inside the tunnel for internal blast loading has rarely been discussed. In the present study, response of rock tunnel subjected to internal blast loading has been investigated. Moreover, Coupled-Eulerian–Lagrangian (CEL) method has been used for the modelling of TNT explosive and air inside the tunnel. Hence, response of rock tunnels under blast loading with CEL method of modelling has rarely been studied. The material behaviour of the TNT has been incorporated through Jones–Wilkins–Lee (JWL) method of equation of state (EOS) which had been neglected in previous studies. Furthermore, a comparative study has been carried out to correlate the damage caused by internal blast loading and the unconfined compressive strength (UCS) of the rock.

2 Modelling and analysis

The present study investigates the effect of UCS of rock on the induced damage of unlined shallow tunnel subjected to blast loading through three-dimensional finite element analyses. Subsequently, a relationship has been developed and proposed to understand intensity of induced damage of rock tunnel subjected to blast loading. For the analysis, a finite element software Abaqus/Explicit has been used [39, 40]. The range of UCS of surrounding rock medium considered in the present study varies in the range of 2.85–207.03 MPa. UCS values considered in the present study represent the strength characteristics mainly of dolomite, shale, sandstone, granite, basalt and quartzite as surrounding medium of tunnel. The properties of these rock mediums are given in Table 1. This section briefly describes the different details of numerical modelling procedure, i.e. geometric domain of numerical model, constitutive model material and solution algorithm.

2.1 The geometry of the tunnel

The finite element model of the rock tunnel has dimensions of 30 m × 30 m in cross section and 35 m in longitudinal direction which represents the length. Moreover, the diameter of the tunnel is taken as 5 m. The geometry of the tunnel model is shown in Fig. 1. The tunnel has 12.5 m of overburden depth and therefore, the boundary of the model lies more than 2.5 d (where d is the diameter of the tunnel, 2.5 d = 2.5 × 5 m = 12.5 m). The geometry of the model has been adopted based on geometry convergence study. C3D8R type of element available in Abaqus library has been used for meshing of the rock surrounding the tunnel. The elements can be defined as an 8-noded brick element with reduced integration and hourglass control. Based on the mesh convergence study, the elements size

Table 1 Input properties of different rocks

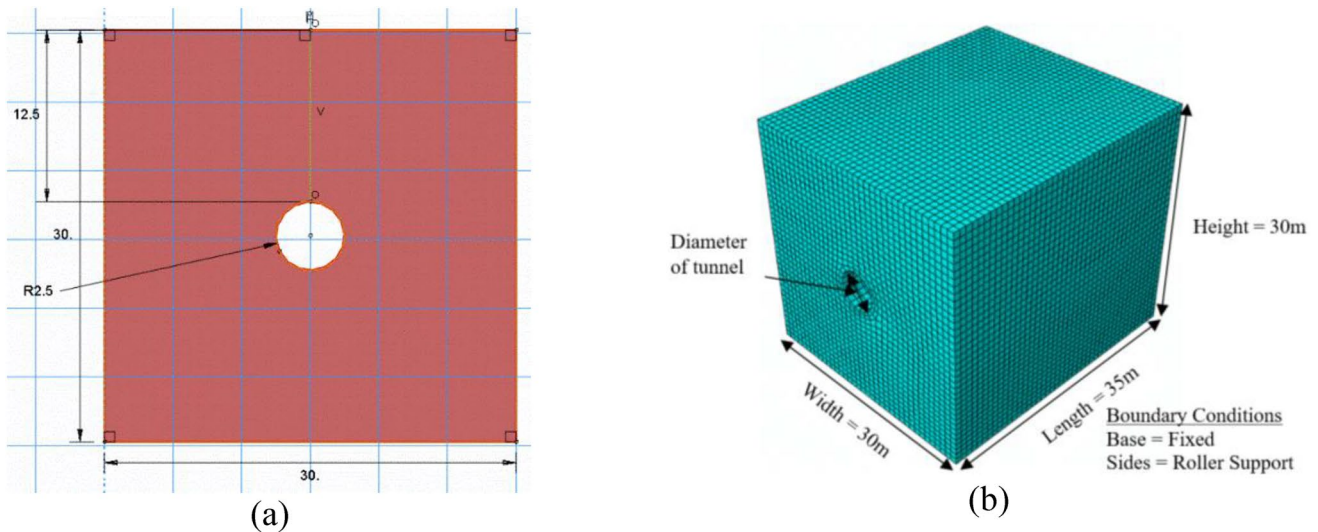|	Density (kg/m³)	Young's modulus (GPa)	Poisson's ratio	Cohesion (MPa)	Angle of friction	UCS(MPa)	Reference
Dolomite	2160	8.12	0.230	0.336	25.22	2.85	[33]
Shale	2550	12.50	0.250	1.600	27.00	50.90	[42]
Sandstone	2300	17.20	0.200	3.300	64.00	86.00	[35]
Granite	2750	36.80	0.187	25.230	58.32	132.80	[36–41]
Basalt	2960	46.50	0.187	26.250	63.38	172.55	[44, 45]
Quartzite	2680	93.80	0.185	27.130	65.30	207.03	–

Fig. 1 **a** Geometry—cross section and **b** meshing of the tunnel model

of the rock has 0.8 mesh size, which divides the model in finite elements. Further, the interaction has been assigned by using general contact interaction property as general hard contact and tangential direction contact as frictionless. Fixed boundary conditions have been applied at the bottom of the model and roller support which allows only in-plane movement has been applied at all sides of the model, while top surface is free to move in any directions. Tunnel surface allows to move in all three translational directions.

2.2 Constitutive material model

Three-dimensional finite element analysis has been carried out in the present study to investigate the response of underground shallow unlined tunnels in rock medium subjected to blast load. Elastoplastic behaviour of the rock has been considered adopting Mohr–Coulomb constitutive material model, which is based on the assumption that failure occurs when maximum shear stress value is
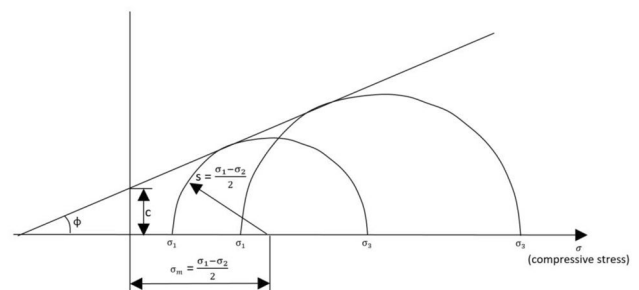

Fig. 2 Mohr–Coulomb yield criterion

reached [15, 39, 40]. This shear stress depends linearly on the normal stress and both lie in the same plane. The failure envelope of the material results in Mohr circle extracted from the triaxial test. The failure envelope gives the value of cohesion and angle of internal friction. The Mohr–Coulomb criterion (as shown in Fig. 2) is given by:

$$\text{Shear strength } (\tau) = \text{ Cohesion } (c) + [\text{normal stress } (\sigma) \, x \, (\tan(\text{internal friction angle } (\phi))). \qquad (1)$$

The Mohr–Coulomb model is represented as three stress invariants for general stress state

$$F = R_{mc}q - p\tan\phi - c = 0, \qquad (2)$$

where

$$R(\Theta, \phi) = \frac{1}{\sqrt{3}\cos\phi}\sin\left(\Theta + \frac{\pi}{3}\right) + \cos\left(\Theta + \frac{\pi}{3}\right)\tan\phi \qquad (3)$$

$$\cos(3\Theta) = \left(\frac{r}{q}\right)^3 \qquad (4)$$

$$p = -\frac{1}{3}trace(\sigma) \qquad (5)$$

$$q = \sqrt{\frac{3}{2}(S:S)} \qquad (6)$$

$$r = (9(S*S:S))^3 \qquad (7)$$

$$S = \sigma + pI, \qquad (8)$$

where S = deviatoric stress. r = third invariant of deviatoric stress. q = Mises equivalent stress. p = equivalent pressure stress. Θ = Deviatoric polar angle.

Moreover, the Mohr–Coulomb yield surface has another term called the flow potential G is defined as

$$G = \sqrt{\left(\epsilon c|_0 \tan\psi\right)^2 + \left(R_{mw}q\right)^2} - p\tan\psi, \qquad (9)$$

where

$$R_{mw}(\Theta, e) = \frac{4\left(1 - e^2\right)\cos^2\Theta + (2e - 1)^2}{2\left(1 - e^2\right)\cos\Theta + (2e - 1)\sqrt{4\left(1 - e^2\right)\cos^2\Theta + 5e^2 - 4e}}R_{mc}\left(\frac{\pi}{3}, \phi\right) \qquad (10)$$

and

$$R_{mc}\left(\frac{\pi}{3}, \phi\right) = \frac{3 - \sin\phi}{6\cos\phi}, \qquad (11)$$

where $c|_0 = c|_\epsilon pl = 0$, ϵ is meridional eccentricity, which explains the rate at which the hyperbolic function approaches the asymptote (this is taken as 0.1 in the present analysis).

$c|_0$ = initial cohesion yield stress.

ψ = dilation angle measured in the $p - R_{mc}$ plane at a high confining pressure.

e = deviatoric eccentricity, which is given as

$$e = \frac{3 - \sin\phi}{3 + \sin\phi}. \qquad (12)$$

The non-associated flow rule has been considered in the present study.

2.3 Blast loading

For simulation of the internal blast-loading event within the tunnel in the present study, the TNT explosive has been modelled using Coupled-Eulerian–Lagrangian (CEL) method. The main advantage of CEL method is that it takes into account the advantages of both, Eulerian and Lagrangian models. Therefore, the general problem of element distortion in finite element analysis in case of dynamic analyses has been eliminated by using CEL method. The CEL method of modelling has been carried out using Eulerian volume fraction (EVF) tool, which is available in Abaqus/Explicit module. EVF option allows the user to specify the amount of material to be filled in the Eulerian part of the model. The range of EVF is 0.0–1.0. EVF = 0.0 means that there is no material and the Eulerian part is empty. However, EVF = 1.0 means that Eulerian part of the model is filled with material and there are no available voids. In the present case of blast loading, the trinitrotoluene (TNT) and the air inside the tunnel have been modelled through CEL method using EVF option. The TNT has EVF = 1.0, which means filled (completely) and no voids, whereas EVF = 0.8 has been used for filling the air inside the tunnel having 20% of voids. The reason for adopting the EVF = 0.8 is that it allows interaction between air and rock material within the tunnel which realistically simulates the condition of blast loading, while EVF = 1.0 represents no interaction of inside air with tunnel during blasting. The TNT explosive has been modelled using JWL-EOS model. This analysis has used CEL modelling technique along with JWL-EOS. The TNT has been assumed to be placed at the centre of the tunnel and by assigning the properties of the TNT. Initially, properties of TNT were assigned to a sphere and placed at the centre of tunnel. Finally, after completing the modelling and meshing, the CEL technique has been used to incorporate large deformations caused by blast loading. The different amounts of

explosive mass considered in this study are, 50 kg, 100 kg, 150 kg, 200 kg, 250 kg and 300 kg. Moreover, the analyses have been carried out for 30 ms, subsequently the response has been discussed. Jones–Wilkins–Lee (JWL) material model has been used for TNT and the input parameters are shown in Table 2. Jones–Wilkins–Lee (JWL) equation of state (EOS) [47] is defined as:

$$p = A\left(1 - \frac{\omega}{R_1 \bar{\rho}}\right)e^{-R_1\bar{\rho}} + B\left(1 - \frac{\omega}{R_2 \bar{\rho}}\right)e^{-R_2\bar{\rho}} + \omega\rho e_{int}, \quad (13)$$

where p = pressure of TNT explosive. A, B, R_1, R_2 and ω are material constants for TNT explosive. Parameters A and B represent the magnitudes of pressure. $\bar{\rho} = \frac{\text{the density of the explosive in the solid-state}}{\text{the current density}}$ e_{int} = specific internal energy at atmospheric pressure.

3 Validation

Validation has been carried out based on available experimental and numerical study of the reinforced cement concrete (RCC) slab having size 1 m × 1 m in plan and 0.4 m of thickness [48]. The RCC slab was reinforced with 6 mm diameter steel bars in both the direction with a spacing of 75 mm centre to centre having 20 mm clear cover. The amount of TNT explosive used is 0.2 kg, 0.31 kg and 0.46 kg at a scaled distance of 0.684 m/kg$^{1/3}$, 0.591 m/kg$^{1/3}$ and 0.518 m/kg$^{1/3}$, respectively. In the present study CEL, method of modelling has been used for the TNT and air. The properties of the steel and RCC adopted in the present case are the same as reported in the literature [48]. The results obtained in the simulation are shown in Table 3 and Fig. 3. The experimental study was carried out for three different TNT explosive charges and the results were validated using finite element software using CEL method by [48]. The sides of the slab were restrained by fixed a boundary and the same was applied in the numerical analysis carried out by [48]. The present validation has also been carried out by considering all the similar loading and boundary conditions.

Table 3 Validation of blast loading

Weight of explosive charge (kg)	Scaled distance (m/kg$^{1/3}$)	Deformation at the centre of the panel (mm)		
		[45]		Present paper
		Experimental study	Numerical study	Numerical study
0.20	0.684	10	8.8	8.32
0.31	0.591	15	12.7	12.37
0.46	0.518	35	31.1	30.57

4 Effect of strain rate

Blast analysis of rock tunnel is a dynamic problem, need to be conducted through strain-dependent material model. However, the open literature doesn't have dynamic material parameters for each rock due to less availability of Split-Hopkinson Pressure Bar test facilities at research institutes. Furthermore, the finite element package Abaqus doesn't have Hoek–Brown Criterion and Dynamic Mohr–Coulomb in its material library. Hence, under these limitations, authors have used strain rate-dependent Drucker–Prager model to conduct a comparative analysis of quartzite rock tunnel. For having an insight into the strain rate effect, a strain rate-dependent simulation has been carried out. All remaining conditions of the rock tunnel under blast loading has been kept constant, in this section. Both Mohr–Coulomb and Ducker Prager model properties have been employed from the literature [46, 49]. The comparative results of the simulation for the Mohr–Coulomb and Ducker–Prager model have been plotted. Figure 4 (a, b and c) shows deformation, stress and acceleration along the length of the tunnel, respectively, for both models. It has been observed that the results obtained through Mohr–Coulomb material model are in acceptable limits, in the present study. Therefore, in the remaining part of the manuscript, Mohr–Coulomb parameters of different rocks have been adopted in the analysis.

5 Results and analysis

The numerical analyses are carried out using Abaqus/Explicit software for the present finite element study of internal blast loading. In this paper, the effect of

Table 2 JWL parameters for TNT explosive

Density (kg/m^3)	Detonation wave speed (m/s)	A (MPa)	B (MPa)	ω	R_1	R_2	Detonation energy density (kJ/kg)
1630	6930	373,800	3747	0.35	4.15	0.9	3680

(a)

(b)

(c)

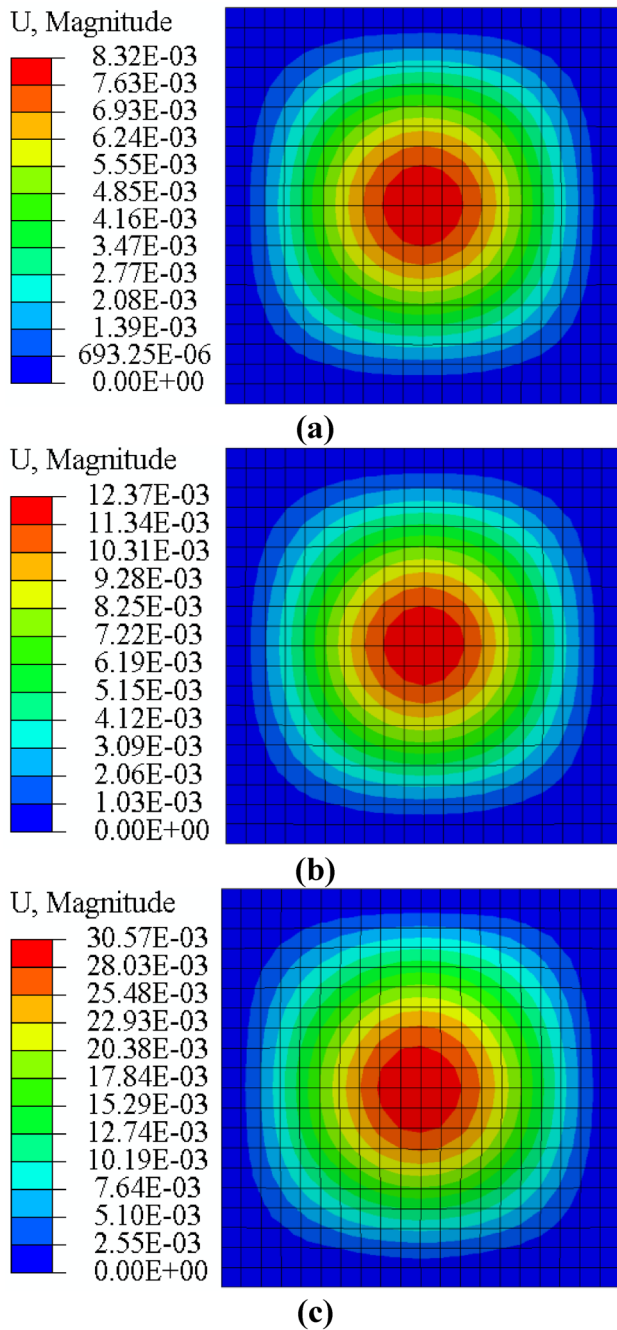**Fig. 3** Numerical results of blast loading on RCC slab for **a** 0.2 kg, **b** 0.31 kg and **c** 0.46 kg TNT explosive
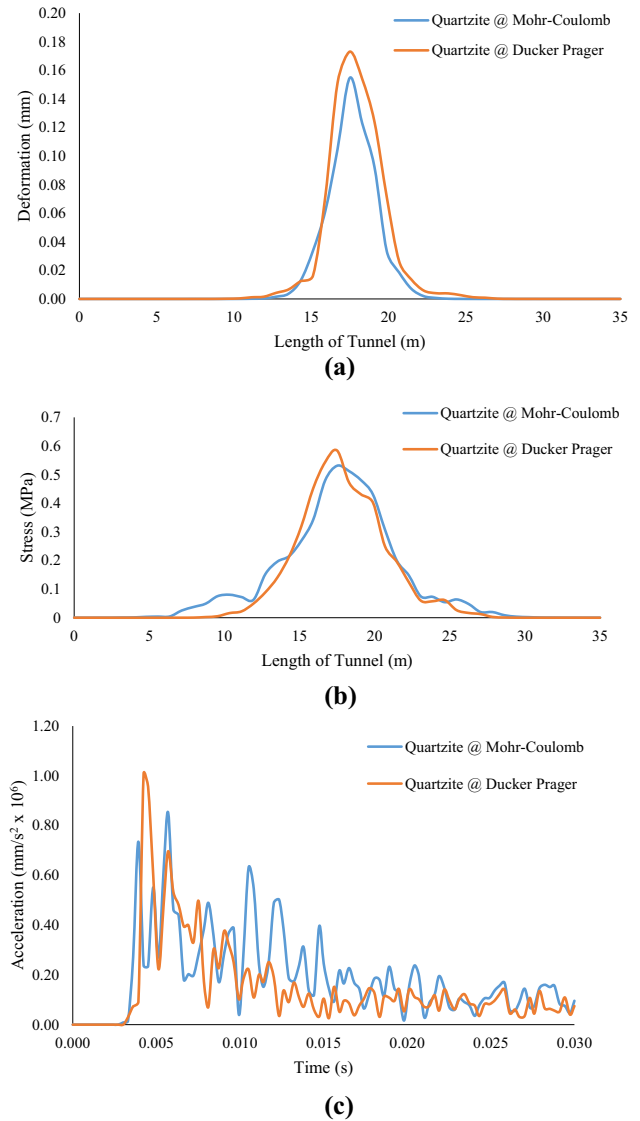

(a)

(b)

(c)

Fig. 4 a Deformation profile of quartzite tunnel under 100 kg of blast loading for comparison of strain rate effect. **b** Variation of stresses along the tunnel length under 100 kg of blast load for quartzite tunnel. **c** Variation of acceleration with time under 100 kg of blast load for quartzite tunnel

unconfined compressive strength (UCS) of the rock surrounding the tunnel has been studied. The trinitrotoluene (TNT) has been modelled using Jones–Wilkins–Lee model in equation of state (EOS) terms. The assumed amount of charge (TNT) for dynamic numerical analysis is 50 kg, 100 kg, 150 kg, 200 kg, 250 kg and 300 kg.

Figure 5 shows the displacement behaviour of different rock tunnels with time when subjected to blast loading.

Dolomite rock tunnel has maximum disturbances with time and least disturbed rock is the quartzite. Moreover, the disturbances in the rock tunnel increase with the decrease in the UCS of rock; therefore, disturbance in the rock tunnel is inversely proportional to the UCS of the surrounding rock. It has been observed that the maximum deformation occurred at 5 ms and due to elastic recovery in strain, it has been minimized later on.

The displacement contours in the different rock tunnels are shown in Fig. 6, for the dynamic load due to blast event. The maximum displacement observed for dolomite,

Fig. 5 Variation of displacement with time for the comparison of different rock tunnels for 100 kg TNT explosive blast load
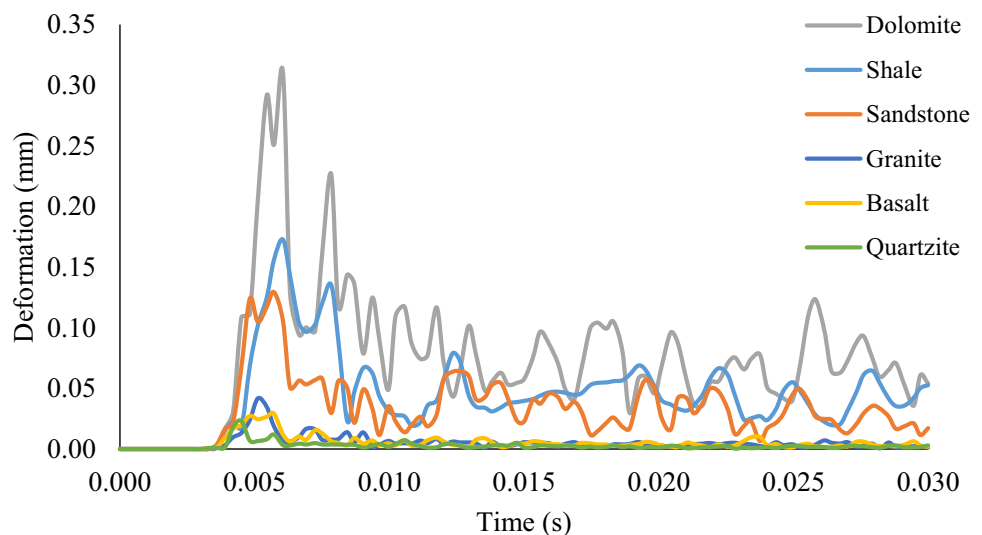
shale, sandstone, granite, basalt and quartzite rock tunnels is 0.883 mm, 0.443 mm, 0.251 mm, 0.045 mm, 0.043 mm and 0.028 mm, respectively. Therefore, among all cases, the maximum and minimum displacement at the tunnel surface has been observed for dolomite and quartzite rock tunnel, respectively. Hence, quartzite rock tunnels are more resistant to blast than the dolomite rock tunnels.

The behaviour of different rocks is compared by plotting the displacement profile along the length of the tunnel, as shown in Fig. 7. As observed earlier, the maximum deformed length has been observed in the case of dolomite rock tunnel, the tunnel constructed in quartzite rock is the most stable case, and maximum deformation concentration has been observed near the blasting event. Therefore, the location of the blast event in the rock tunnel has a significant role in the deformation pattern.

Figure 8 is plotted for concluding the effect of UCS of the stability of the rock tunnel. Hence, it has been concluded that UCS of the rock surrounding the tunnel is exponentially related to the maximum deformation observed in the tunnel when subjected to internal blast loading. Therefore, the deformation in the tunnel and the UCS of the rock are related as given by Eq. (14).

$$y \propto e^{-x}, \tag{14}$$

where x is the value of UCS of rock surrounding the tunnel in MPa and y is the displacement in the tunnel in mm.

Homogeneity, strength and resistance of the rock are the governing parameters for the energy dissipation in the rock [50]. The induced energy is dissipated in the form of heat energy, surface energy and plastic energy when the blast waves propagate through the surrounding rocks [51]. In the present study, the input/incident is constant due to the fixed amount of charge. Hence, the rock with

kinetic energy value has lower potential energy, which in turn may be interpreted as instability of the structure. Figure 9 shows the total energy plot with time for different rocks. The maximum total energy noted for dolomite, shale, sandstone, granite, basalt and quartzite rock tunnel is 218 MJ, 47.1 MJ, 87.9 MJ, 85.9 MJ, 84.9 MJ and 81.4 MJ, respectively. It had been reported that for a confined rock blasting [52]. The values measured for each of the kinetic energy would be 3–21% of the total energy available. Figure 10 shows the kinetic energy with time of different rocks. The maximum kinetic energy has been observed in the case of dolomite rock. Figure 11 is plotted to depict the acceleration variation in different rocks under 100 kg of blast loading. It has been observed that the maximum vibrations are transferred in case of quartzite rock due to its maximum brittle behaviour. In addition, a drastic reduction in acceleration has been observed for basalt rock.

6 Discussion

Coupled-Eulerian–Lagrangian modelling technique proves to be a useful tool for analysis of blast-induced loading. It overcomes the problem of excessive element distortion. Peak deformation is significantly higher for the rocks having lower UCS values. UCS, angle of friction and cohesion contributes to the stability of the tunnel. Moreover, granite, basalt and quartzite possess higher value of UCS and show negligible amount of deformations under similar conditions as compared to rock tunnels in dolomite, shale and sandstone. The propagation of the shear wave/blast wave causes a minimum effect in the dolomite and quartzite tunnel hence proved to be the most resistant to blast loading due to explosion. Deformation magnitude reaches the maximum value at a fixed time depending on UCS of
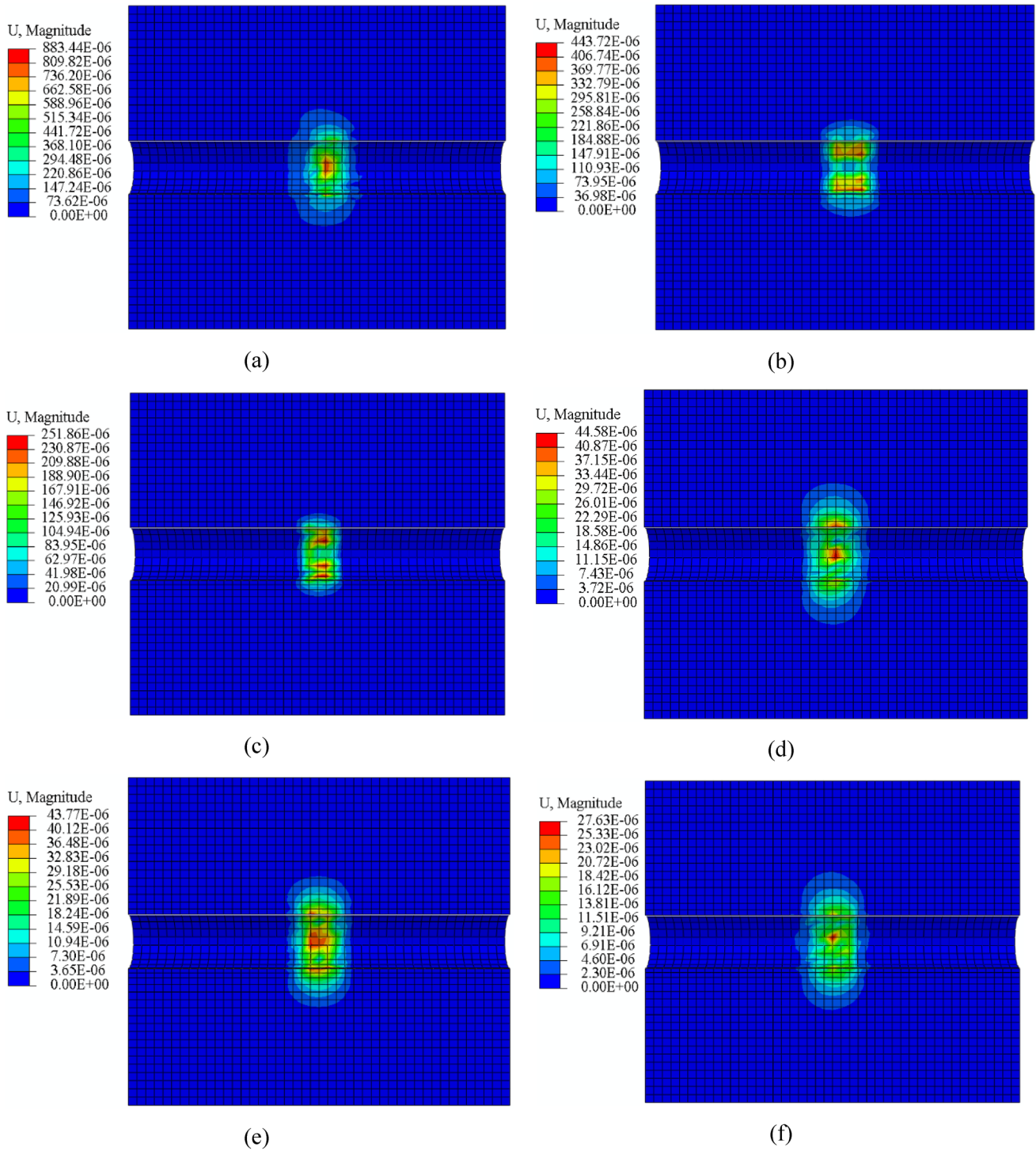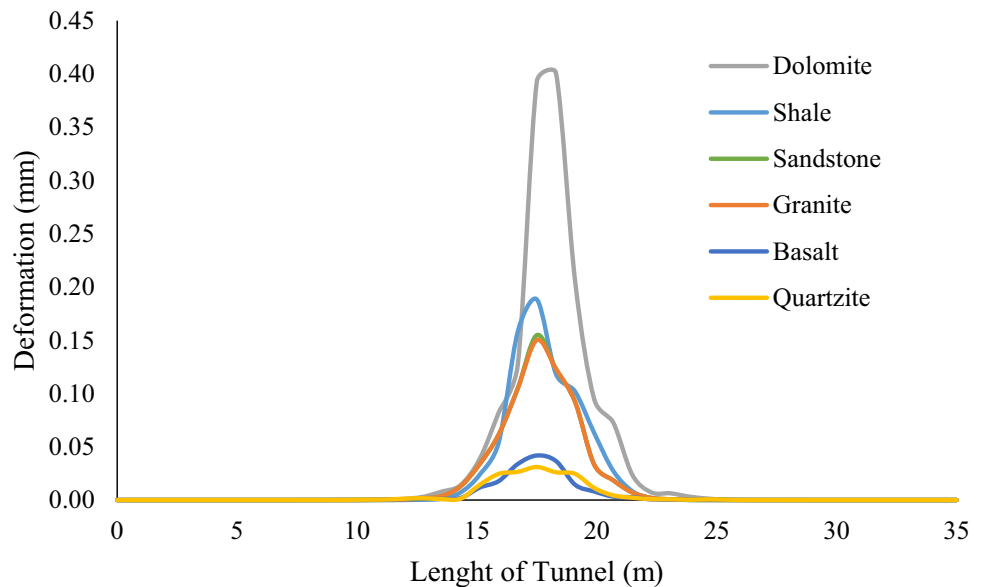
Fig. 6 The displacement (m) contours of **a** dolomite, **b** shale, **c** sandstone, **d** granite, **e** basalt and **f** quartzite rock tunnel for 100 kg TNT explosive blast load

Fig. 7 Displacement profile along the length of the tunnel for different rocks for 100 kg TNT explosive blast load

the rock and then it diminishes. It has also been concluded that the relation between the deformation and the UCS of rock is exponential. The total energy and kinetic energy value of the rock significantly depends on the inherent properties of the rock and UCS of the rock governs magnitude of total and kinetic energy. The result of this study suggests that the designing of the tunnel should consider the UCS of the rock and the support of the tunnel must be categorized based on UCS of the rock. The rocks can be divided into two groups; a value of UCS greater than 100 MPa and less than 100 MPa. Further, each category has been subdivided as "Higher", "Intermediate" and "Lower". Therefore, this paper proposed a new method of tunnel support categorization and classification.

7 Conclusion

Dynamic analysis of the tunnel in rock with different UCS of rock has been analysed here and different observations are presented. Three-dimensional finite element analyses of the rock tunnel subjected to blast loading have been performed using Coupled-Eulerian–Lagrangian (CEL) modelling technique. The model has been validated against published data in the literature and dynamic response of tunnel die to blast-induced loading for different UCS

values of rock has been investigated. The explosive and air surrounding the explosive inside the tunnel have been modelled using Eulerian elements. Maximum deformation, propagation of waves, acceleration response, location of blasting have been investigated and presented. The paper may be useful for the researchers and practicing engineers working in the area of tunnel engineering. Following conclusions are drawn based on the results and observations made in this paper.

1. The magnitude of the deformation in the dolomite tunnel is 99% higher than shale. Similarly, shale has 76% higher than sandstone, sandstone has 4.65-times higher than granite, granite has 2% higher than basalt and basalt has 58% higher than quartzite.
2. Rock having a higher value of UCS shows lower magnitude of deformation and is the safest from stability consideration cases of the tunnel. The peak displacement and the extent of damage are inversely proportional to the UCS in the rock tunnel when subjected to internal blast loading.
3. The kinetic energy generated and total energy absorbed in the rock due to blast loading are inversely proportional to the UCS of the rock; therefore, higher energy has been absorbed by dolomite and a lesser

Fig. 8 Effect of UCS of rock for the deformation in the tunnel in case of **a** the different amounts of explosives and **b** 3D plot for combined effect
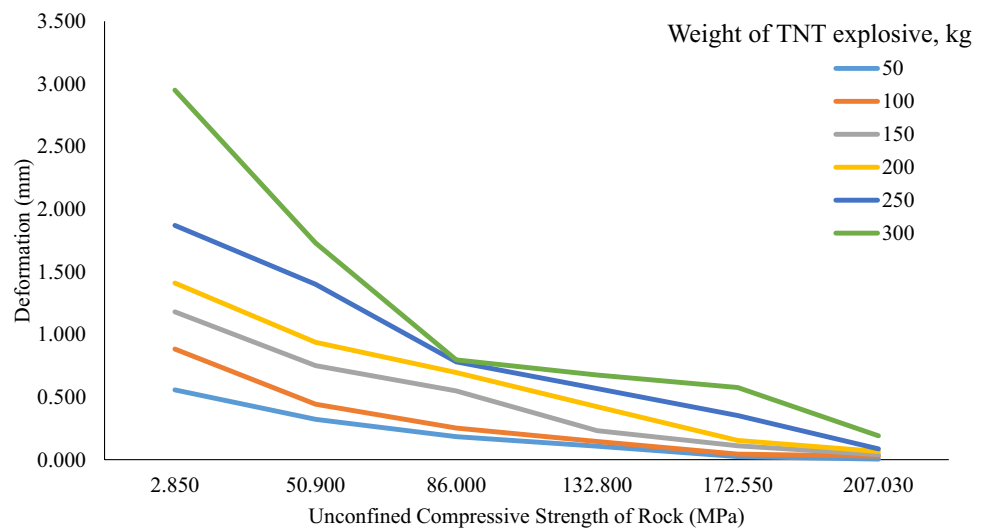
(a)
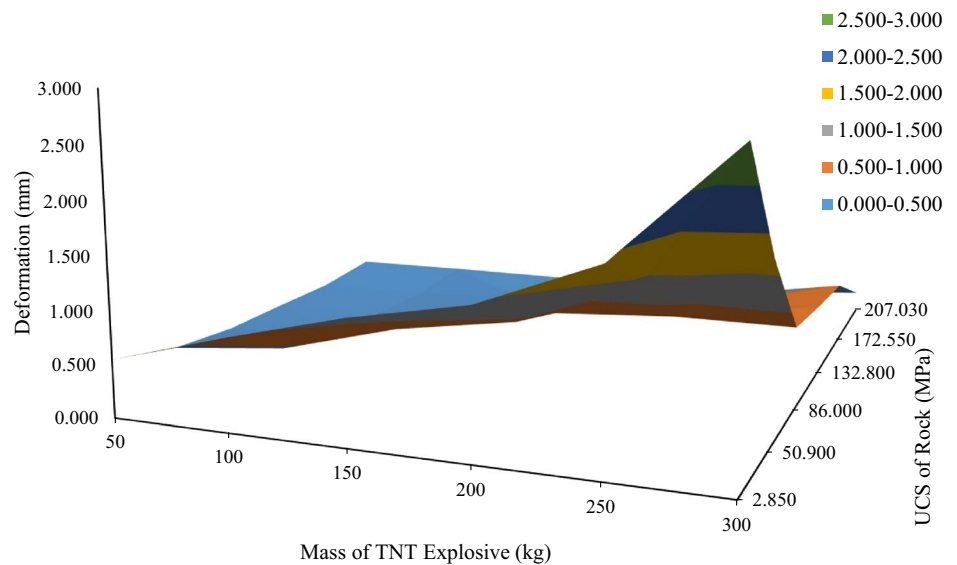
(b)

amount of energy has been generated and absorbed in quartzite tunnel.

4. The overall safety of the tunnel is higher in quartzite, basalt and granite in comparison with dolomite, shale and sandstone tunnel.

5. For the present study, dolomite and quartzite having the lowest and highest UCS suffer maximum and minimum deformation, respectively, as observed for the input parameters considered in the present study.

However, a large number of rocks should be considered for development of a more rational relation between UCS of rock and other relatable parameters for blast resistant design approach of rock tunnel.

Fig. 9 Variation of total energy with time for different rocks for 100 kg TNT explosive blast load
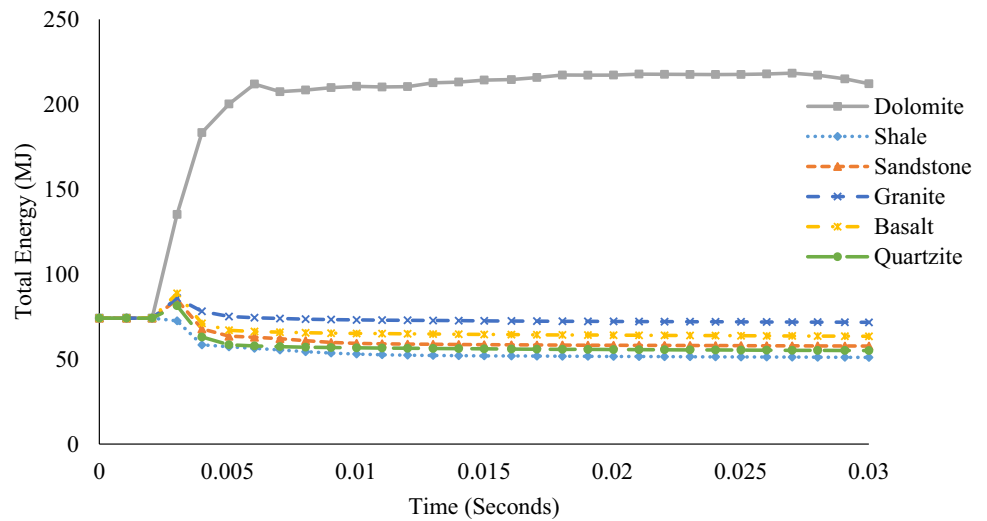

Fig. 10 Variation of kinetic energy in case of different rocks with time for 100 kg TNT explosive blast load
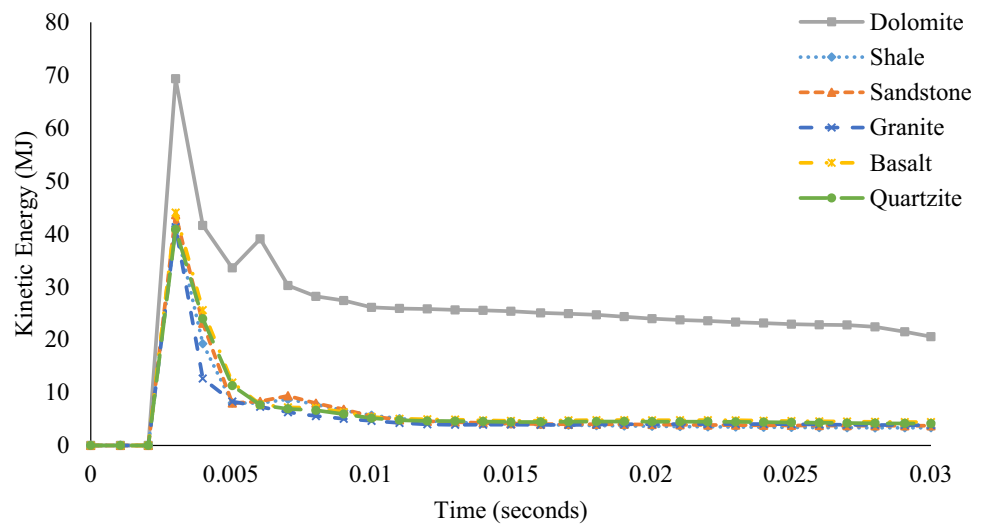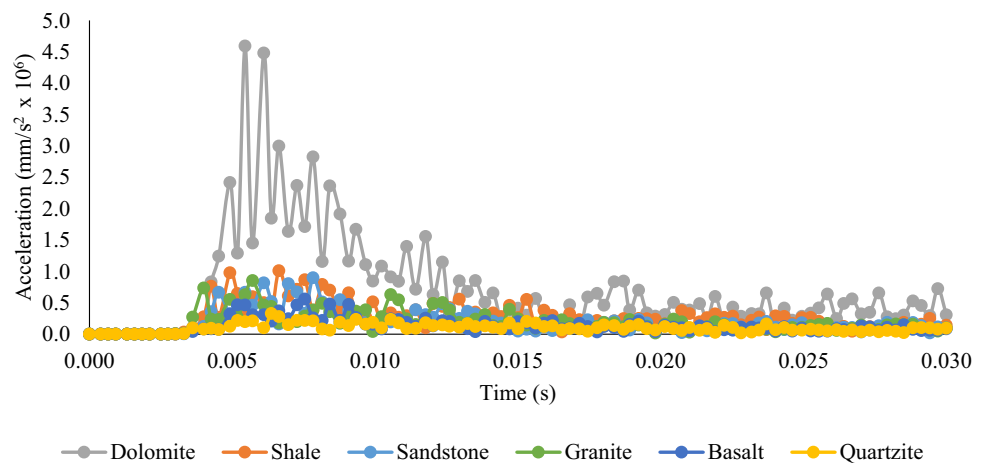

Fig. 11 Comparison of acceleration obtained at the crown of tunnel when subjected to 100 kg of blast load

Compliance with ethical standards

Conflict of interest   Authors declare that they have no potential conflict of interest.

References

1. Bangash M, Bangash T (2005) Explosion-resistant buildings: design, analysis and case studies. Springer, Berlin
2. Hoffman B, Reinares F (2014) The evolution of the global terrorist threat: from 9/11 to Osama bin Laden's death. Columbia University Press, Columbia
3. Chaudhary RK, Mishra S, Chakraborty T, Matsagar V (2019) Vulnerability analysis of tunnel linings under blast loading, Int J Prot Struct 10 73 94 https://doi.org/10.1177/2041419618789438
4. Chakraborty T, Larcher M, Gebbeken N, Khas H, Mechanics S (2014) Performance of tunnel lining materials under internal blast loading. Int J Prot Struct 5:83–96. https://doi.org/10.1260/2041-4196.5.1.83
5. Tiwari R, Chakraborty T, Matsagar V (2020) Analysis of curved tunnels in soil subjected to internal blast loading. Acta Geotech 15:509–528. https://doi.org/10.1007/s11440-018-0694-x
6. Naqvi MW, Zaid M, Sadique MR, Alam MM (2017) Dynamic analysis of rock tunnels considering joint dip angle : a finite element approach, in: 13th Int. Conf. Vib. Probl., Indian Institute of Technology Guwahati, India
7. Zaid M, Rehan Sadique M (2021), Dynamic analysis of tunnels in western ghats of Indian peninsula: effect of shape and weathering, in: recent trends Civ. Eng., Springer, Singapore: pp. 763–776. https://doi.org/https://doi.org/10.1007/978-981-15-5195-6_57
8. Jian-po L, Chang-yin Z, Ying-tao S, Ren W, Gang L, Shi-da X (2020) Temporal-spatial evolution of acoustic emission during progressive fracture processes around tunnel triggered by blast-induced disturbances under uniaxial and biaxial compression. Tunn Undergr Sp Technol 96:103229. https://doi.org/10.1016/j.tust.2019.103229
9. Fang XQ, Zhang TF, Li BL, Yuan RJ (2020) Elastic-slip interface effect on dynamic stress around twin tunnels in soil medium subjected to blast waves. Comput Geotech 119:103301. https://doi.org/10.1016/j.compgeo.2019.103301
10. Zaid M, Sadique MR (2020a) Blast resistant behaviour of tunnels in sedimentary rocks. Int J Prot Struct. https://doi.org/10.1177/2041419620951211
11. Zaid M, Athar MF, Sadique MR (2019) Effect of rock weathering on the seismic stability of different shapes of the tunnel, in: Indian Geotech. Conf., SVNIT, Surat, India
12. Zaid M, Naqvi MW, Sadique MR (2019) Stability of Arch Tunnel in Different Magnitude of Earthquake with Effect of Weathering in Western Ghats of India, in: Indian Geotech. Conf., SVNIT, Surat, India
13. Athar MF, Zaid M, Sadique MR (2019) Stability of different shapes of tunnels in weathering stages of Basalt, in: Proc Natl Conf Adv Struct Technol, NIT Silchar, pp. 320–327
14. Zaid M, Mishra S, Rao KS (2019) Stability of different shapes of Himalayan tunnels under blast loading, in: 8th Indian Rock Conf., New Delhi pp. 375–380
15. Zaid M, Sadique MR (2020b) The response of rock tunnel when subjected to blast loading: finite element analysis. Eng Reports. https://doi.org/10.1002/eng2.12293
16. Kristoffersen M, Minoretti A, Børvik T (2019) On the internal blast loading of submerged floating tunnels in concrete with circular and rectangular cross-sections. Eng Fail Anal 103:462–480. https://doi.org/10.1016/j.engfailanal.2019.04.074
17. Tian X, Song Z, Wang J (2019) Study on the propagation law of tunnel blasting vibration in stratum and blasting vibration reduction technology. Soil Dyn Earthq Eng 126:105813. https://doi.org/10.1016/j.soildyn.2019.105813
18. Yang G, Wang G, Lu W, Yan P, Chen M (2019) Damage assessment and mitigation measures of underwater tunnel subjected to blast loads. Tunn Undergr Sp Technol 94:103131. https://doi.org/10.1016/j.tust.2019.103131
19. Liu H (2009) Dynamic analysis of subway structures under blast loading. Geotech Geol Eng 27:699–711. https://doi.org/10.1007/s10706-009-9269-9
20. Feldgun VR, Karinski YS, Yankelevsky DZ (2014) The effect of an explosion in a tunnel on a neighboring buried structure. Tunn Undergr Sp Technol 44:42–55. https://doi.org/10.1016/j.tust.2014.07.006
21. Liu H (2011) Damage of cast-iron subway tunnels under internal explosions, in: Geotech. Spec. Publ. pp. 1524–1533. https://doi.org/10.1061/41165(397)156
22. Ng CWW, Liu GB, Li Q (2013) Investigation of the long-term tunnel settlement mechanisms of the first metro line in Shanghai. Can Geotech J 50:674–684. https://doi.org/10.1139/cgj-2012-0298
23. Han Y, Zhang L, Yang X (2016) Soil-tunnel Interaction under Medium Internal Blast Loading, in: Procedia Eng., Elsevier Ltd, pp. 403–410. https://doi.org/https://doi.org/10.1016/j.proeng.2016.06.051
24. Naqvi MW, Akhtar MF, Zaid M, Sadique MR (2020) Effect of superstructure on the stability of underground tunnels. Transp Infrastruct Geotechnol. https://doi.org/10.1007/s40515-020-00119-6
25. Shi C, Zhao Q, Lei M, Peng M (2019) Vibration velocity control standard of buried pipeline under blast loading of adjacent tunnel. Soils Found 59:2195–2205. https://doi.org/10.1016/j.sandf.2019.12.003
26. Zaid M, Md Sadique R (2020) Numerical modelling of internal blast loading on a rock tunnel. Adv Comput Des 5:4. https://doi.org/10.12989/acd.2020.5.4.417
27. Zaid M, Sadique Md R, Masroor M, Alam Samanta M (2020) Effect of shear zone on dynamic behaviour of rock tunnel constructed in highly weathered granite. Geomech Eng 23(3):245–259. https://doi.org/10.12989/gae.2020.23.3.245
28. Liu H (2012) Soil-structure interaction and failure of cast-iron subway tunnels subjected to medium internal blast loading. J Perform Constr Facil 26:691–701. https://doi.org/10.1061/(ASCE)CF.1943-5509.0000292
29. Han Y, Zhang L, Yang X (2016) Soil-tunnel interaction under medium internal blast loading. Procedia Eng 143:403–410. https://doi.org/10.1016/j.proeng.2016.06.051
30. Osinov VA, Chrisopoulos S (2020) Two neighbouring tunnels in saturated soil under blast loading, in: Recent Dev Soil Mech Geotech Theory Pract, Springer, Cham, pp. 281–296. https://doi.org/https://doi.org/10.1007/978-3-030-28516-6_15
31. Han Y, Yang X, Ni J (2020) Influence of foam liner on tunnels subjected to internal blast loading, in: Lect. Notes Electr. Eng., Springer, pp. 1373–1378. https://doi.org/https://doi.org/10.1007/978-981-15-0644-4_103
32. Zhou Q, He guang H, Liu feng S, Chen shuo X, Tang xun Z, Liu Y, Qiu yu Z, Li sen S, Wang H, Zhou zhi Y, Zhou nan J, Fan lin H, Jin nian F (2020) Blast resistance evaluation of urban utility tunnel reinforced with BFRP bars. Def Technol. https://doi.org/10.1016/j.dt.2020.03.015
33. Tiwari R, Chakraborty T, Matsagar V (2016a) Dynamic analysis of a twin tunnel in soil subjected to internal blast loading. Indian Geotech J 46:369–380. https://doi.org/10.1007/s40098-016-0179-5

34. Deng XF, Zhu JB, Chen SG, Zhao ZY, Zhou YX, Zhao J (2014) Numerical study on tunnel damage subject to blast-induced shock wave in jointed rock masses. Tunn Undergr Sp Technol 43:88–100. https://doi.org/10.1016/j.tust.2014.04.004

35. Tiwari R, Chakraborty T, Matsagar V (2016b) Dynamic analysis of tunnel in weathered rock subjected to internal blast loading. Rock Mech Rock Eng 49:4441–4458. https://doi.org/10.1007/s00603-016-1043-8

36. Deng XF, Zhu JB, Chen SG, Zhao J (2012) Some fundamental issues and verification of 3DEC in modeling wave propagation in jointed rock masses. Rock Mech Rock Eng 45:943–951. https://doi.org/10.1007/s00603-012-0287-1

37. Zhu JB, Li YS, Wu SY, Zhang R, Ren L (2018) Decoupled explosion in an underground opening and dynamic responses of surrounding rock masses and structures and induced ground motions: A FEM-DEM numerical study. Tunn Undergr Sp Technol 82:442–454. https://doi.org/10.1016/j.tust.2018.08.057

38. Deng XF, Chen SG, Zhu JB, Zhou YX, Zhao ZY, Zhao J (2014) UDEC–AUTODYN hybrid modeling of a large-scale underground explosion test Rock Mech Rock Eng 48:737–747. https://doi.org/10.1007/s00603-014-0600-2

39. Hibbitt D, Karlsson B, Sorensen P (2014) ABAQUS user-manual release 6.14. Dassault Systèmes Simulia Corp, RI

40. Systemes D (2014) Abaqus 6.14 documentation. Dassault Systèmes, RI

41. Kumar A (2019) Engineering behavior of oil shale under high pressure after thermal treatment. IIT, Delhi

42. Gschwandtner GG, Galler R (2013) Laugungsversuche als Grundlage zur Stabilitätsuntersuchung von Grubengebäuden in wasserlöslichen GebirgsformationenLeaching experiments as basis for the stability analysis of underground structures in water-soluble rock formations. BHM Berg-Und Hüttenmännische Monatshefte 158:493–500. https://doi.org/10.1007/s00501-013-0202-4

43. Gahoi A, Zaid M, Mishra S, Rao KS (2017) Numerical analysis of the tunnels subjected to impact loading, in: 7th Indian Rock Conf, Indorock2017, New Delhi

44. Zaid M, Mishra S, Rao KS (2020) Finite element analysis of static loading on urban tunnels. In: Latha Gali M, P RR (eds) Geotechnical characterization and modelling. Lecture notes in civil engineering, vol 85. Springer, Singapore. https://doi.org/10.1007/978-981-15-6086-6_64

45. Mitelman A, Elmo D (2014) Modelling of blast-induced damage in tunnels using a hybrid finite-discrete numerical approach. J Rock Mech Geotech Eng 6:565–573. https://doi.org/10.1016/j.jrmge.2014.09.002

46. Gupta AS (1997) Engineering behavior and classification of weathering rock. Indian institute of technology, Delhi

47. Larcher M, Casadei F (2010) Explosions in complex geometries—a comparison of several approaches. Int J Prot Struct 1:169–195. https://doi.org/10.1260/2041-4196.1.2.169

48. Zhao CF, Chen JY (2013) Damage mechanism and mode of square reinforced concrete slab subjected to blast loading. Theor Appl Fract Mech 63–64:54–62. https://doi.org/10.1016/j.tafmec.2013.03.006

49. Yadav HR (2005) Geotechnical evaluation and analysis of Delhi metro tunnels. Indian Institute of Technology, New Delhi

50. Song D, Wang E, Li Z, Liu J, Xu W (2015) Energy dissipation of coal and rock during damage and failure process based on EMR. Int J Min Sci Technol 25:787–795. https://doi.org/10.1016/j.ijmst.2015.07.014

51. Lu CP, Dou LM (2014) The relationship between vertical stress gradient, seismic and electromagnetic emission signals at Sanhejian coal mine, China. Int J Rock Mech Min Sci 70:90–100. https://doi.org/10.1016/j.ijrmms.2014.04.010

52. Sanchidrián JA, Segarra P, López LM (2007) Energy components in rock blasting. Int J Rock Mech Min Sci 44:130–147. https://doi.org/10.1016/j.ijrmms.2006.05.002